



## Revisiting the stability of 2D passive biped walking: Local behavior

James A. Norris\*, Anthony P. Marsh, Kevin P. Granata, Shane D. Ross

Virginia Tech-Wake Forest University, School of Biomedical Engineering & Sciences, One Medical Center Drive WFUHS, MC-1022 27157-1022 Winston-Salem, NC, United States

### ARTICLE INFO

#### Article history:

Received 12 September 2007

Received in revised form

21 June 2008

Accepted 2 July 2008

Available online 22 July 2008

Communicated by V. Rom-Kedar

#### Keywords:

Compass walker

Passive dynamic walking

Gait

Dynamic stability

Piecewise-holonomic

Hybrid dynamical system

### ABSTRACT

Models of biped walking have demonstrated that stable walking motions are possible without active control. Stability of these motions has typically been quantified by studying the stability of an associated Poincaré map (orbital stability). However, additional insight may be obtained by examining how perturbations evolve over the short-term (local stability). For example, there may be regions where small perturbations actually diverge from the unperturbed trajectory, even if over the entire cycle small (but perhaps not large) perturbations are dissipated. We present techniques to calculate local stability, and demonstrate the utility of these techniques by examining the local stability of the 2D compass biped. These techniques are relevant to the design of controllers to maintain stability in robots, and in understanding how the neuromuscular system maintains stability in humans.

© 2008 Elsevier B.V. All rights reserved.

### 1. Introduction

Passive dynamic models of biped walking have proven useful in understanding generalized principles that govern walking motions [1–9]. The term passive dynamics arises from the ability of these models to walk without active control. To replace the energy lost in foot impacts and friction, these models walk down a slight slope. McGeer was the first to show that a walking motion actually emerges as a stable periodic cycle from the dynamic equations governing a simple planar model [1]. More recently, Collins, et al., built a more complicated physical model, not restricted to planar motion, that also walks down a slope and very closely resembles human walking [8]. The beauty of these devices is that their energy consumption is very low, and that they exhibit dynamically stable walking motions. This approach to studying walking has been adopted by both the robotics community, where the aim is to design robots that are as versatile and efficient as humans, and the biomechanics community, where the goal is to improve our understanding of walking.

One of the most important factors for successful walking is stability [10]. In fact, the physical models and robots that have been designed around passive dynamic walkers are very susceptible to small disturbances; as openly admitted by their designers, who tend to remain within arms reach at all times. To date, analysis

of stability has focused primarily on stability of step-to-step, or Poincaré, maps. Poincaré maps are useful for determining if a periodic cycle exhibits orbital stability. This approach, however, misses the rich dynamic behavior in the neighborhood of the solution trajectory. For example, there may be regions where perturbations diverge from the solution trajectory, referred to as local instability, and other regions where perturbations are attracted back to the solution, local stability. In fact, orbital stability (or instability) results from the competition of these local tendencies integrated over the cycle [11].

The goal of this study was to characterize the changing local dynamic stability of a passive dynamic model of walking. Moreover, we expanded techniques designed for analyzing local stability of continuous periodic cycles to handle walking models, which often include continuous dynamics, coupled with a discrete event to approximate foot-strike collisions. One advantage of calculating local stability is the ability to quantify the time-varying vector direction of instability in state space, and identify phases of the walking cycle that may be more susceptible to disturbances. For the robotics community, understanding local stability will be useful in designing controllers to maintain stability. Local stability is also relevant to biomechanists and clinicians interested in instability and falling in older adults and clinical populations (e.g. diabetic peripheral neuropathy, vestibular disorders) because of the potential to identify individuals with poorer stability at all phases of the walking cycle, who may be at greater risk for falling.

\* Corresponding address: Creare Inc., 16 Great Hollow Road, PO Box 71, Hanover, NH 03755, United States. Tel.: +1 603 643 3800; fax: +1 603 643 4657.

E-mail addresses: [jan@creare.com](mailto:jan@creare.com), [jesse.a.norris@gmail.com](mailto:jesse.a.norris@gmail.com) (J.A. Norris).

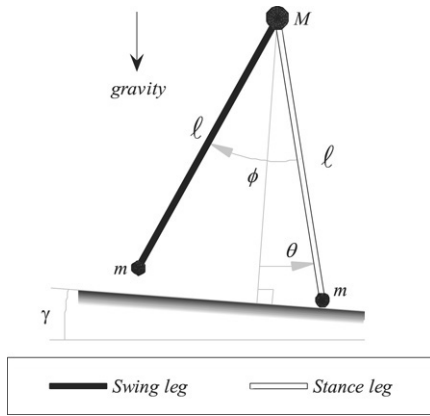


**Fig. 1.** Two-segment walker with hip mass,  $M$ , weightless legs, and point masses at the feet,  $m$ .

## 2. Model

The model explored in this paper is the 2D compass biped with point feet (Fig. 1). It consists of two mass-less legs connected at the hip, a point mass at the hip,  $M$ , and a point mass at each foot,  $m$ . This model walks down a rigid surface at a slope of  $\gamma$ . The walking cycle is composed of a swing phase, where the stance foot does not slip, and behaves like a pin joint, and an instantaneous double-stance phase when the swing foot strikes the ground. At foot-strike, we assume an inelastic collision brings the swing foot to rest, and calculate the angular velocities after foot-strike, by conservation of angular momentum. Thus, the solution requires a two-part approach of (A) solving the continuous swing-phase equations until a foot-strike occurs, and (B) applying the instantaneous conservation of momentum equations. Following the foot-strike event, stance- and swing-states are swapped before continuing with steps (A–B) for a subsequent step. This section concludes with the techniques used to find periodic solutions (C).

### 2.1. Swing phase equations of motion

Defining the mass ratio between foot and hip mass,  $\beta = m/M$ , and rescaling time by  $\sqrt{\ell/g}$ , the non-dimensional equations describing the motion of the biped walker are only functions  $\beta$  and  $\gamma$ ,

$$\begin{aligned} & \begin{bmatrix} 1 - 2\beta(\cos\phi - 1) & \beta(\cos\phi - 1) \\ \beta(\cos\phi - 1) & \beta \end{bmatrix} \begin{bmatrix} \ddot{\theta} \\ \ddot{\phi} \end{bmatrix} \\ & + \begin{bmatrix} -\beta(\dot{\phi}^2 - 2\dot{\theta}\dot{\phi})\sin\phi \\ -\beta\dot{\theta}^2\sin\phi \end{bmatrix} \\ & + \begin{bmatrix} (1 + \beta)\sin(\gamma - \theta) - \beta\sin(-\theta + \phi + \gamma) \\ \beta\sin(-\theta + \phi + \gamma) \end{bmatrix} = \begin{bmatrix} 0 \\ 0 \end{bmatrix} \end{aligned} \quad (1)$$

where  $\theta$  is the angle of the stance leg with respect to the normal of the inclined plane, and  $\phi$  is the angle between the legs (Fig. 1). These two, second order equations may be reorganized as a set of four first-order equations in Hamiltonian form. This may be achieved by defining momenta coordinates,  $p_\theta$  and  $p_\phi$ , according to,

$$\begin{bmatrix} p_\theta \\ p_\phi \end{bmatrix} = \begin{bmatrix} 1 - 2\beta(\cos\phi - 1) & \beta(\cos\phi - 1) \\ \beta(\cos\phi - 1) & \beta \end{bmatrix} \begin{bmatrix} \dot{\theta} \\ \dot{\phi} \end{bmatrix}. \quad (2)$$

Defining the state  $\mathbf{s} = [\theta \ \phi \ p_\theta \ p_\phi]^T$ , these two second-order differential equations may be expressed as a set of four nonlinear first-order equations, (see Box 1). These four first-order swing-phase equations represent a typical initial value problem, and may be solved numerically, given an initial state.

Since this system is conservative, we are guaranteed that the Hamiltonian energy is constant during swing-phase. This is one of the reasons it is desirable to express the equations in Hamiltonian form. The Hamiltonian energy,  $H(\mathbf{s})$ , is:

$$H(\mathbf{s}) = (1 + \beta)\cos(\gamma - \theta) - \beta\cos(\gamma - \theta + \phi) + \frac{p_\theta^2 + (2 - 2\cos\phi)p_\theta p_\phi + (2 - 2\cos\phi + \beta^{-1})p_\phi^2}{2 + 2\beta\sin^2\phi}. \quad (3)$$

### 2.2. Foot-strike transition equations

Foot-strike occurs when the swing leg has passed in front of the stance leg and the inter-leg angle is exactly twice the stance leg angle,  $\phi - 2\theta = 0$ . At this event, the swing-phase numerical integration is halted, and an impulsive inelastic collision brings the swing foot to rest. We assume no impulsive forces act on the former stance foot as it leaves the ground [1,7]. To calculate the angular velocities after the foot-strike collision, we apply conservation of angular momentum about the new stance foot for the entire system, and about the hip for the new swing foot. Furthermore, since the impulse is assumed to occur instantaneously, the stance and inter-leg angles are constant. Additionally, to prepare for the next step, the states are swapped as part of the foot-strike transition. The transition from pre (– superscript) to post (+ superscript) may then be described by a linear operator,

$$\begin{aligned} \mathbf{s}^+ &= \begin{bmatrix} \theta \\ \phi \\ p_\theta \\ p_\phi \end{bmatrix}^+ = \begin{bmatrix} 1 & -1 & 0 & 0 \\ 0 & -1 & 0 & 0 \\ 0 & 0 & \frac{\cos\phi}{1 + \beta\sin^2\phi} & \frac{\cos\phi(1 - \cos\phi)}{1 + \beta\sin^2\phi} \\ 0 & 0 & 0 & 0 \end{bmatrix} \\ &\times \begin{bmatrix} \theta \\ \phi \\ p_\theta \\ p_\phi \end{bmatrix}^- = \mathbf{G}(\mathbf{s}^-). \end{aligned} \quad (4)$$

This matrix is for the more general case where  $\phi - 2\theta$  is not required to be zero, which might arise from walking over an irregular surface, and is used for tracking a disturbance across the foot-strike event (see Section 3.4). When foot-strike satisfies  $\phi - 2\theta = 0$ , we may reduce this matrix to a rank 2 matrix,

$$\begin{aligned} \mathbf{s}^+ &= \begin{bmatrix} \theta \\ \phi \\ p_\theta \\ p_\phi \end{bmatrix}^+ = \begin{bmatrix} 0 & -\frac{1}{2} & 0 & 0 \\ 0 & -1 & 0 & 0 \\ 0 & 0 & \frac{\cos\phi}{1 + \beta\sin^2\phi} & \frac{\cos\phi(1 - \cos\phi)}{1 + \beta\sin^2\phi} \\ 0 & 0 & 0 & 0 \end{bmatrix} \\ &\times \begin{bmatrix} \theta \\ \phi \\ p_\theta \\ p_\phi \end{bmatrix}^- = \mathbf{G}(\mathbf{s}^-). \end{aligned} \quad (5)$$

### 2.3. Walking solutions

For the model to walk, there must be a solution to the swing-phase (continuous) and foot-strike (discrete) equations that is a non-stationary solution for all time, e.g. a periodic cycle, a quasi-periodic cycle, or a chaotic attractor. Interestingly, it has been generally accepted that for a given parameter set, if a stable solution exists, there will be one and only one stable solution [2,7]. Previous research has considered walking solutions as fixed points of the Poincaré section measured at the foot-strike event [1,2,4,7].

$$\dot{\mathbf{s}} = \begin{bmatrix} \frac{p_\theta + (1 - \cos \phi) p_\phi}{1 + \beta \sin^2 \phi} \\ \frac{p_\phi + \beta (1 - \cos \phi) (p_\theta + 2p_\phi)}{\beta (1 + \beta \sin^2 \phi)} \\ -(1 + \beta) \sin(\gamma - \theta) + \beta \sin(\gamma - \theta + \phi) \\ -\beta \sin(\gamma - \theta + \phi) + \frac{\sin \phi (p_\theta + (1 - \cos \phi) p_\phi (\beta \cos \phi p_\theta - (1 + \beta - \beta \cos \phi) p_\phi))}{(1 + \beta \sin^2 \phi)^2} \end{bmatrix} = \mathbf{F}(\mathbf{s})$$

Box I.

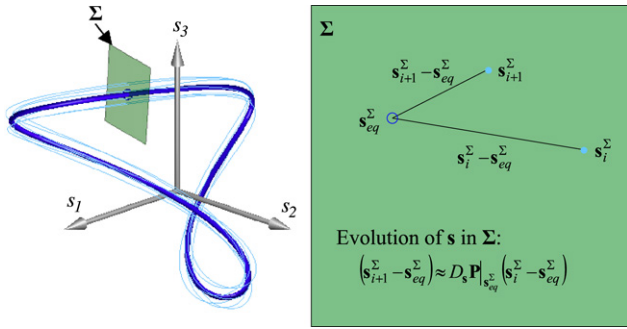


**Fig. 2.** Left: Equilibrium solution,  $\mathbf{s}_{eq}(t)$ —dark blue, and perturbed solutions shown in light blue. Right: Intersection of a perturbed solution,  $\mathbf{s}_i^\Sigma$ , and its subsequent intersection,  $\mathbf{s}_{i+1}^\Sigma$ , with the Poincaré section,  $\Sigma$ . (For interpretation of the references to colour in this figure legend, the reader is referred to the web version of this article.)

Poincaré sections are constructed from a hypersurface in the state-space that is transverse to the solution of the continuous-time dynamics (Fig. 2). Our Poincaré section is the three-dimensional hypersurface,  $\Sigma$ , given by  $\phi - 2\theta = 0$ . The relationship between a previous,  $\mathbf{s}_i^\Sigma$ , and a subsequent,  $\mathbf{s}_{i+1}^\Sigma$ , intersection of the solution with this hypersurface is expressed as a Poincaré map,  $\mathbf{P}$ ,

$$\mathbf{s}_{i+1}^\Sigma = \mathbf{P}(\mathbf{s}_i^\Sigma) \quad (6)$$

where the superscript  $\Sigma$  denotes that the state is in the hypersurface  $\Sigma$ . One possible walking solution is for the current step to exactly match the subsequent step,  $\mathbf{s}_{eq}^\Sigma = \mathbf{P}(\mathbf{s}_{eq}^\Sigma)$ . This equilibrium solution,  $\mathbf{s}_{eq}^\Sigma$ , represents a periodic (period-one) solution and is a fixed point of the map. Higher period solutions may also exist, and represent solutions of the form  $\mathbf{s}_{eq}^\Sigma = \mathbf{P}^k(\mathbf{s}_{eq}^\Sigma)$ , where  $k$  is the number of steps before returning to the equilibrium solution [12].

Taking the Poincaré section at the instant of foot-strike reduces the search space from four dimensions to two. This is a consequence of the geometry, which requires that the inter-leg angle is twice that of the stance leg angle. Moreover, by concentrating mass at the feet, the post-foot-strike momentum coordinate,  $p_\phi$ , is always zero. Period-one walking solutions were found numerically using the MATLAB function *fminsearch*. The MATLAB function *ode45* was used to numerically integrate the swing phase dynamic equations. Additional techniques for finding walking solutions are discussed in [1,7,13].

### 3. Stability of biped walking

To date, stability analysis has focused largely on analyzing the stability of fixed points of the Poincaré map. This type of stability analysis is useful for determining whether the equilibrium solution exhibits orbital stability. For example, if all solutions that intersect the Poincaré section near the fixed point return to the fixed point on subsequent steps, then the equilibrium solution exhibits orbital asymptotic stability (Fig. 2). Conversely,

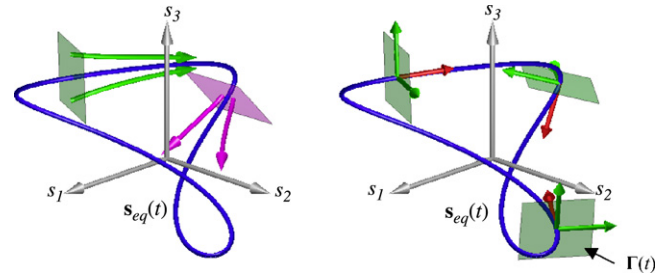


**Fig. 3.** Left: Locally stable region (green) and unstable (magenta) along a trajectory  $\mathbf{s}_{eq}(t)$ . Right: Examples of the locally rotating reference frame defined by the tangent direction (red) and orthogonal directions (green) spanning the orthogonal hypersurface  $\Gamma(t)$ . (For interpretation of the references to colour in this figure legend, the reader is referred to the web version of this article.)

if upon subsequent steps intersections with the Poincaré section diverge from the fixed point, the equilibrium solution is unstable. Orbital stability reduces the question of stability of a periodic orbit to the stability of a fixed point of an associated discrete map. This reduction, however, ignores potentially useful stability information along the equilibrium solution, when it is between Poincaré intersections. For example, there may be regions along the equilibrium solution where perturbed solutions will tend to diverge from the equilibrium solution (local instability) and regions where perturbed solutions will converge back to the equilibrium solution (local stability) (Fig. 3). Orbital stability (or instability) results from these competing local tendencies averaged over the entire cycle [11].

We first briefly review a numerical technique that has been previously used to calculate orbital stability for the biped walker (A). In B and C, the local stability during swing phase is derived. Section D is devoted to how foot-strike collision affects stability. Lastly, we demonstrate how orbital stability may be calculated from the local stability measures for this hybrid continuous-discrete system (E).

#### 3.1. Orbital dynamic stability

Orbital stability of a given walking solution may be quantified by calculating eigenvalues of an estimated Jacobian of the Poincaré map. First, a periodic solution for a given slope,  $\gamma$ , and mass ratio,  $\beta$ , is found numerically. Next, evolution of two linearly independent perturbation vectors about the fixed point are tracked forward to their subsequent intersections with the Poincaré section. Since the foot-strike event is rank two, perturbations need only be two-dimensional, but they must be in the hypersurface  $\Sigma$ . Integration of the swing-phase equations requires the full four dimensions. One map between two possible perturbation coordinates and the full four dimensional state is the 2 by 4 matrix  $\mathcal{E}$ ,

$$\mathcal{E} = \begin{bmatrix} 1 \cdot 5^{-1/2} & 2 \cdot 5^{-1/2} & 0 & 0 \\ 0 & 0 & 1 & 0 \end{bmatrix} \text{ and}$$

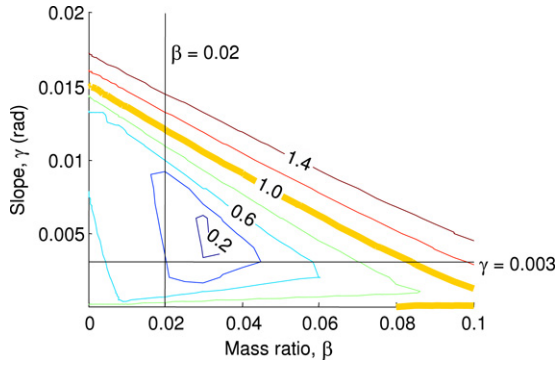


**Fig. 4.** Maximum of the absolute value of eigenvalues of the estimated Jacobian for period-one solutions for combinations of slope,  $\gamma$ , and mass ratio,  $\beta$ . Period-one solutions are stable where this plot is below one. The two dash-dot lines show the slices of this parameter space that are presented in Figs. 6 and 7.

$$\begin{bmatrix} \delta_\theta \\ \delta_\phi \\ \delta_{p_\theta} \\ \delta_{p_\phi} \end{bmatrix} = \mathbf{E}^T \cdot \begin{bmatrix} \delta_{\Sigma_1} \\ \delta_{\Sigma_2} \end{bmatrix} \quad \text{and} \quad (7)$$

where  $\delta_\Sigma$  are perturbations in the two-dimensional frame.

An estimate of the Jacobian of the Poincaré map for the fixed point may then be obtained from,

$$D_s \mathbf{P}|_{s_{eq}} \approx \mathbf{A}_f^\Sigma \cdot (\mathbf{A}_0^\Sigma)^{-1} \quad (8)$$

where  $\mathbf{A}_f^\Sigma$  and  $\mathbf{A}_0^\Sigma$  are  $2 \times 2$  matrices of the final perturbation vectors after integration of the swing equations and discrete foot-strike event, and the initial perturbation vectors in  $\Sigma$ , respectively. If the absolute value of any eigenvalue of the estimated Jacobian is greater than one, perturbed solutions will eventually diverge from the equilibrium. Thus, the equilibrium solution is considered unstable. When all the eigenvalues are inside the unit circle, subsequent intersections converge to the equilibrium and asymptotic stability is achieved.

Fig. 4 shows the maximum of the absolute value of the eigenvalues of the estimated Jacobian for period-one solutions for the parameters  $\beta$  and  $\gamma$ . Orbital stability is achieved where the maximum of the eigenvalue magnitudes is less than one. Period-one walking cycles are a symmetric walk, i.e. the left and right leg steps are identical. As the model is sent down steeper slopes, the stable walking pattern bifurcates to a period-two, then a period-four walking cycle, and so on until the stable attractor appears chaotic [2,4,7].

### 3.2. Local dynamic stability

For a dynamic system described by,

$$\dot{\mathbf{s}} = \mathbf{F}(\mathbf{s}) \quad (9)$$

let  $\mathbf{s}_{eq}(t)$  be a periodic orbit that includes the fixed point,  $\mathbf{s}_{eq}^\Sigma$ , of the Poincaré map. Further, let  $\mathbf{s}_{eq}(t) + \delta(t)$  be a perturbed trajectory. Substituting the perturbed trajectory into Eq. (9) and assuming the perturbation is initially small such that its evolution may be described by linearization about the equilibrium trajectory, we find,

$$\dot{\delta}(t) = D_s \mathbf{F}|_{s_{eq}(t)} \cdot \delta(t) \quad (10)$$

where  $D_s \mathbf{F}|_{s_{eq}(t)}$  is the Jacobian of  $\mathbf{F}$  evaluated along the periodic solution,  $\mathbf{s}_{eq}(t)$ . The local rate of expansion (or contraction) of a volume in the state-space, which describes and constrains the short-time evolution of all possible perturbed trajectories about  $\mathbf{s}$ , is given by the divergence of the flow,

$$\bar{\nabla} \cdot \mathbf{F} = \text{div } \mathbf{F}(\mathbf{s}) = \text{trace}(D_s \mathbf{F}) = \sum_{i=1}^n \frac{\partial \dot{s}_i}{\partial s_i} = \sum_{i=1}^n \lambda_i \quad (11)$$

where  $\lambda_i$  are the eigenvalues of the Jacobian of  $\mathbf{F}$ .

Since swing-phase is a conservative system, in canonical Hamiltonian form, we are guaranteed that the divergence of  $\mathbf{F}$  is zero. It should be noted, however, that zero divergence is not guaranteed for other state-space coordinate frames, for instance coordinates and velocities, and is an important reason for choosing conjugate coordinate-momentum pairs as state-space variables. Zero divergence does not guarantee stability, as unstable periodic orbits are found in many examples of autonomous Hamiltonian systems of two or more degrees of freedom. This is due to the fact that in Hamiltonian systems, stable and unstable directions come in pairs, yielding overall instability even though their rates balance to give a divergence of zero [14].

### 3.3. Vector components of local dynamic stability

Further insight into the local stability is gained by interpreting the individual elements of the Jacobian of  $\mathbf{F}$ . Diagonal elements capture the local divergence (convergence) rates along each state variable direction. Off-diagonal elements indicate rates that couple the perturbations from the other state variable directions. From this point forward, we will refer to divergence and convergence rates simply as divergence rates, recognizing that convergence is the result of a negative divergence rate.

To improve the interpretation of the divergence rates, we change the frame of reference from which perturbations are viewed [11]. One natural transformation is to calculate the eigenvalues,  $\lambda_i(t)$ , and eigenvectors,  $\mathbf{e}_i(t)$ , of  $D_s \mathbf{F}(\mathbf{s})|_{s_{eq}(t)}$ , where  $i = 1, \dots, n$ . This transformation yields the divergence rates at time  $t$ ,  $\lambda_i(t)$ , which are now uncoupled, along the changing eigenvector directions. Furthermore, the linearized solution to Eq. (10) at time  $t$ , describes the short-term time evolution,  $t + dt$ , of the perturbation  $\delta(t)$ ,

$$\delta(t + dt) = \sum_{i=1}^n b_i(t) \mathbf{e}_i(t) \exp(\lambda_i(t) dt) \quad (12)$$

where the  $b_i(t)$  coefficients are determined by the initial condition  $\delta(t)$ . If the real part of  $\lambda_i(t)$  is less than zero for all  $i$ , any perturbation about the point  $\mathbf{s}_{eq}(t)$  is drawn back toward  $\mathbf{s}_{eq}(t)$  in the near future, i.e. in the time interval  $[t, t + dt]$ . Thus, the equilibrium solution is termed locally stable at time  $t$ . Otherwise, the equilibrium solution is locally unstable.

The real and imaginary parts of the four eigenvalues for the swing-phase dynamics are shown in Fig. 5. For all of the swing phase, there is one pair of equal and opposite eigenvalues with only real components, and one conjugate pair of imaginary eigenvalues, as expected for a canonical Hamiltonian system. Since the real part of one eigenvalue is positive throughout swing-phase, the entire swing-phase exhibits one locally unstable direction in the state-space, even though the complete solution with foot-strike may be orbitally stable (Fig. 4). This is an example of global stability of a solution despite local instability [11]. In this case, as opposed to the examples in [11], the global stability arises despite the local instability of the continuous dynamics due to dimension collapse at the discrete foot-strike event, as described in the next section.

Increasing the foot to hip mass ratio ( $\beta$ ), increased both the average and maximum of the magnitudes of the real and imaginary eigenvalues (Fig. 5). Even though the locally unstable direction is balanced by the stable direction such that the divergence is zero, the greater local instability may be one of the reasons why the period-one solutions become orbitally unstable with increasing  $\beta$ .

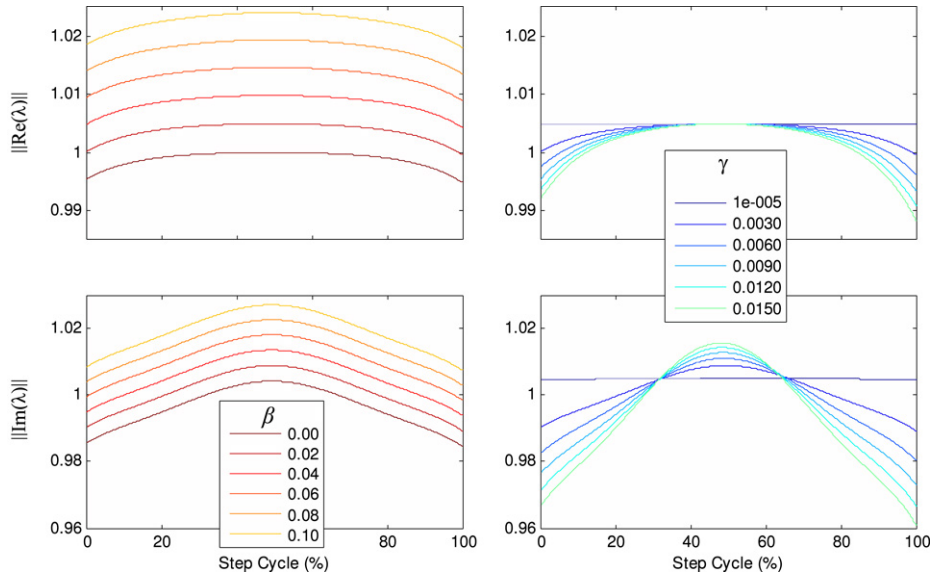


**Fig. 5.** Eigenvalues,  $\lambda$ , of the Jacobian of  $\mathbf{F}(\mathbf{s}(t))$ . There is a pair of purely real eigenvalues with the same magnitude, and a pair of purely imaginary eigenvalues with the same magnitude. For each pair, one eigenvalue is the negative of the other. Dependence of the eigenvalues while varying foot to hip mass ratio,  $\beta$ , (left), and slope,  $\gamma$ , (right).

Increasing the slope ( $\gamma$ ) caused the magnitude of the real eigenvalues to decrease at the beginning and end of swing phase and did not affect the maximum, thus decreasing the average magnitude. For the imaginary components, increasing  $\gamma$  led to decreases at the beginning and end, and an increase in the maximum, which occurred just before 50% of the gait cycle. The net effect on the imaginary components was a decrease in their average magnitude.

Although the divergence rates for each eigenvector direction are uncoupled, this transformation does not take into account the evolution of the underlying periodic orbit. For instance, consider a system where the only eigenvalue that was locally unstable corresponded to an eigenvector direction that was tangent to evolution of the periodic orbit. This local instability would not affect the stability of the walking process; it would simply result in a phase shift. Thus, a convenient reference frame is obtained by rotating to a frame that remains tangent and orthogonal to the equilibrium solution (Fig. 3). Transforming perturbations from the global state basis,  $\delta(t)$ , to this local frame which varies along the solution,  $\delta'(t)$ , may be accomplished through a time-varying unitary rotation matrix,  $\mathbf{U}|_{\text{seq}(t)}$ ,

$$\delta'(t) = \mathbf{U}|_{\text{seq}(t)} \cdot \delta(t) \quad (13)$$

where the evolution of  $\delta'(t)$  is governed by

$$\begin{aligned} \dot{\delta}'(t) &= \left( \mathbf{U} \cdot D_s \mathbf{F} \cdot \mathbf{U}^{-1} + \frac{d\mathbf{U}}{dt} \cdot \mathbf{U}^{-1} \right) \Big|_{\text{seq}(t)} \cdot \delta'(t) \\ &= \mathbf{B}(t) \delta'(t) \\ &= \begin{bmatrix} \lambda_{\tau\tau}(t) & \lambda_{\tau\eta_1}(t) & \cdots \\ \lambda_{\eta_1\tau}(t) & \lambda_{\eta_1\eta_1}(t) & \cdots \\ \vdots & \vdots & \ddots \end{bmatrix} \delta'(t) \end{aligned} \quad (14)$$

where  $\mathbf{B}(t)$  is the stability matrix in this locally rotating frame and the subscripts on  $\lambda$  denote the tangent,  $\tau$ , and normal,  $\eta$ , directions that make up the rotating frame. The first row of the  $\mathbf{U}$  matrix is the unit tangent vector,  $\mathbf{F}(\mathbf{s}(t))^T \cdot \|\mathbf{F}(\mathbf{s}(t))\|^{-1}$ . The remaining rows are unit vectors orthogonal to the tangent vector. There is not a unique set of these orthogonal vectors, as they may be any combination of vectors that form an orthogonal basis in the hypersurface orthogonal to the tangent,  $\Gamma(t)$ . This transformation

results in the  $\lambda_{\eta\tau}(t)$  terms being zero. Thus, a tangent perturbation remains tangent and is uncoupled from the normal directions. The instantaneous rate of expansion of a disturbance volume in  $\Gamma(t)$  is unique and is given by,  $\text{div } \mathbf{F}(\mathbf{s}(t)) - \lambda_{\tau\tau}$ . This rate of expansion is a measure of the rate of divergence of trajectories in  $\Gamma(t)$ . It is important to note that since  $\mathbf{U}$  is a unitary rotation matrix, the matrix  $\frac{d\mathbf{U}}{dt} \cdot \mathbf{U}^{-1}$  is skew-symmetric and therefore traceless. This implies that  $\text{trace}(\mathbf{B}(t)) = \text{trace}(D_s \mathbf{F})$  and therefore the volume divergence rate about a point in state space is independent of the transformation  $\mathbf{U}$ , i.e.,  $\text{div } \mathbf{F}(\mathbf{s}(t)) = \sum \lambda_i = \text{trace}(D_s \mathbf{F}) = \text{trace}(\mathbf{B}(t))$ . This also provides a means to numerically check the  $\mathbf{B}(t)$  matrix. The analytical solution to  $\lambda_{\tau\tau}$  is,

$$\lambda_{\tau\tau} = \frac{\dot{\mathbf{s}}^T \cdot D_s \mathbf{F} \cdot \dot{\mathbf{s}}}{\dot{\mathbf{s}}^T \cdot \dot{\mathbf{s}}} \quad (15)$$

The rate of divergence of trajectories in  $\Gamma(t)$  is presented in Fig. 6 for varying mass ratios,  $\beta$ , and slopes,  $\gamma$ . Additionally, since the tangent direction is now uncoupled from the normal directions, it is possible to look just at the eigenvalues of a reduced matrix that describes evolution of the normal perturbations. This reduced matrix is formed by removing the first column and top row of the  $\mathbf{B}$  matrix. Similar to how the  $n$  eigenvalues of the Jacobian of  $\mathbf{F}$  may be examined to determine local stability in the global state-space, examining the  $(n - 1)$  eigenvalues of this reduced matrix may be used to determine local stability in this orthogonal hypersurface,  $\Gamma(t)$ , Fig. 6. This is ultimately the frame we are interested in using to study stability of walking.

When  $\beta$  is zero, stability in the orthogonal hypersurface differs from physically plausible foot to hip mass ratios,  $\beta > 0$  (Fig. 6). This difference is due to the uncoupling of the swing-foot momenta and gravity terms from the dynamics describing the stance-leg angle,  $\theta$ . For a given mass ratio, however, increasing the slope does not have a large effect on the qualitative behavior of the stability in the orthogonal hypersurface for period-one solutions. When the slope actually is too steep ( $\gamma = 0.015$ ) and the period-one solution is no longer stable (Fig. 4), the stability in the orthogonal hypersurface does not appear to be significantly different than that of the stable period-one solutions.

### 3.4. Local dynamic stability of foot strike event

Up to this point, local stability has been presented for the swing-phase. Swing-phase dynamics are smooth-continuous functions

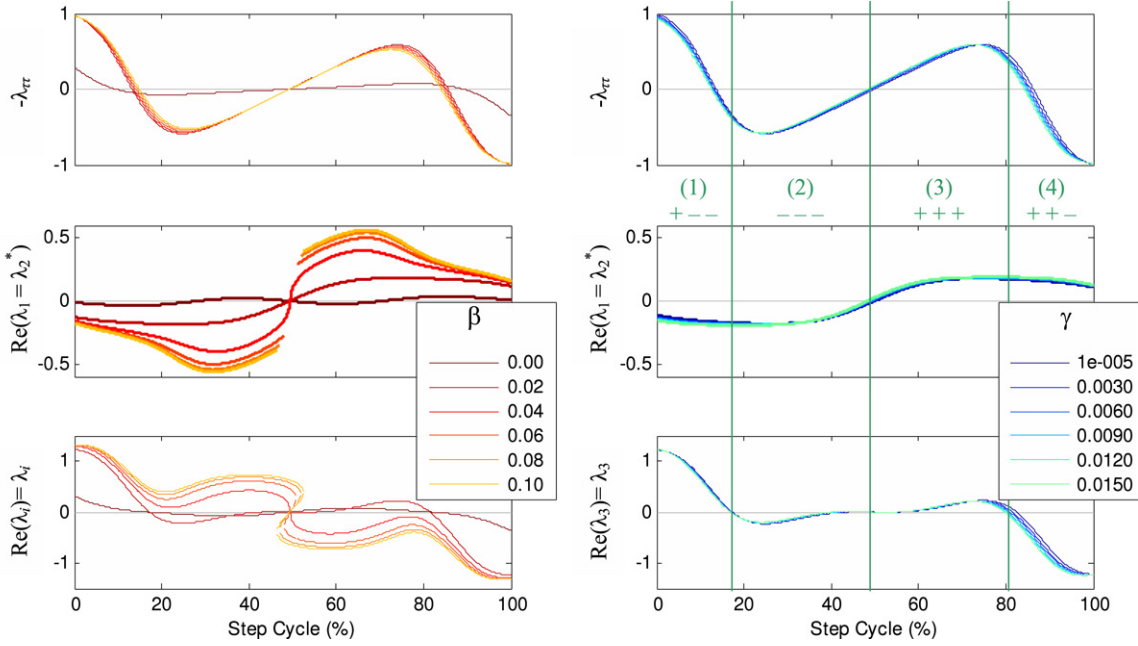


**Fig. 6.** Divergence in the orthogonal hypersurface,  $\text{div } \mathbf{F}(\mathbf{s}(t)) - \lambda_{\tau\tau} = -\lambda_{\tau\tau}$ , while varying foot to hip mass ratio,  $\beta$ , for slope  $\gamma = 0.003$  (left), and varying slope,  $\gamma$ , for mass ratio  $\beta = 0.02$  (right) is shown in the top graphs. The middle and lower graphs are the real parts of the three eigenvalues of the reduced  $\mathbf{B}$  matrix. These eigenvalues capture evolution of perturbations in the rotating orthogonal hypersurface,  $\Gamma(t)$ . The thick lines in the middle graphs indicate a complex conjugate pair of eigenvalues. The break in the middle of the graph on the left shows how increasing  $\beta$  causes the complex conjugate pair of eigenvalues to transition to three eigenvalues with only real elements (in the bottom figure on the left). Generalized behavior for the numbered regions identified in the right graph are diagrammed in Fig. 7.

with respect to time. Impact dynamics of the foot-strike event occur over an infinitesimal amount of time and are not smooth. To determine how the foot-strike event affects a disturbance volume in the state-space, we track a perturbed foot-strike state,  $\mathbf{s}^- + \delta^-$ . The foot-strike equations are of the form  $\mathbf{s}^+ = \mathbf{G}(\mathbf{s}^-)$ , and  $t^+ = t^-$ . Substituting a perturbed foot-strike state into Eq. (4) and retaining terms only to first-order in the disturbance,

$$\begin{aligned} \mathbf{s}^+ + \delta^+ &= \mathbf{G}(\mathbf{s}^- + \delta^-) \\ &= \mathbf{G}(\mathbf{s}^-) + D_s \mathbf{G}(\mathbf{s}^-) \delta^- \\ &= \mathbf{s}^+ + \begin{bmatrix} 1 & -1 & 0 & 0 \\ 0 & -1 & 0 & 0 \\ 0 & \frac{\partial G_3}{\partial \phi} & \frac{\cos \phi}{1 + \beta \sin^2 \phi} & \frac{\cos \phi (1 - \cos \phi)}{1 + \beta \sin^2 \phi} \\ 0 & 0 & 0 & 0 \end{bmatrix} \delta^- \end{aligned} \quad (16)$$

where  $G_3$  is the third element of the  $\mathbf{G}(\mathbf{s}^-)$  vector from Eq. (4). Thus, we are left with the relationship between the pre to post foot-strike perturbations as the Jacobian of the foot-strike map,  $D_s \mathbf{G}(\mathbf{s}^-)$ ,

$$\delta^+ = D_s \mathbf{G}(\mathbf{s}^-) \delta^-. \quad (17)$$

Since this event is discrete, it causes an instantaneous change in the state-space volume perturbations occupy, not a rate of volume change like in the continuous dynamics. The ratio of volume after the event compared to volume before the event is related to the absolute value of the determinant of the Jacobian of  $\mathbf{G}$ ,

$$\text{DIV } \mathbf{G}(\mathbf{s}) = |\det(D_s \mathbf{G})| = |\Lambda_1 \Lambda_2 \cdots \Lambda_n| \quad (18)$$

where  $\Lambda_i$  are the eigenvalues of the Jacobian of  $\mathbf{G}$ . If this ratio is less than unity, then the discrete event  $\mathbf{G}$  causes a contraction of perturbation volume.

The eigenvalues,  $\Lambda$ , of the Jacobian of  $\mathbf{G}$  are

$$\Lambda = \left[ -1, \quad 1, \quad \frac{\cos \phi}{1 + \beta \sin^2 \phi}, \quad 0 \right]. \quad (19)$$

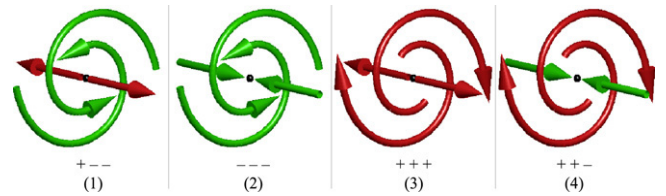


**Fig. 7.** Schematic of divergence in  $\Gamma(t)$ , the hypersurface orthogonal to the trajectory, for the regions identified in Fig. 6. Green (or light gray) arrows are attracting and red (or dark gray) indicate divergence.

Similar to examining the magnitude of the eigenvalues of the estimated Jacobian of the Poincaré map, we may gain understanding of how the foot-strike event affects perturbation magnitude by examining these eigenvalues. The first two eigenvalues with unity magnitude correspond to the fact that the foot-strike event has no effect on perturbations to the stance and inter-leg angles. The magnitude of the third eigenvalue is always less than one for realistic inter-leg angles at the foot-strike event, i.e.  $\phi \neq 0$ . This third eigenvalue corresponds to dissipation of perturbations to the hip-momentum,  $p_\theta$ , at foot-strike. The zero eigenvalue is related to the fact that swing phase momentum is always forced to zero post-foot-strike.

Using the map described in Eq. (7),  $\mathcal{E}$ , it is possible to restrict the Jacobian of  $\mathbf{G}$  to the two perturbation vectors in  $\Sigma$ . This provides insight into the effect  $\mathbf{G}$  has on perturbations, since the rank of  $\mathbf{G}$  is only two, and the zero eigenvalue causes  $\text{DIV } \mathbf{G}(\mathbf{s})$  to be zero. The eigenvalues and  $\text{DIV}$  of this reduced 2 by 2 matrix are,

$$\begin{aligned} \Lambda_{2 \times 2} &= \left[ -1, \quad \frac{\cos \phi}{1 + \beta \sin^2 \phi} \right] \quad \text{and} \\ \text{DIV } \mathbf{G}(\mathbf{s})_{2 \times 2} &= \frac{|\cos \phi|}{1 + \beta \sin^2 \phi}. \end{aligned} \quad (20)$$

As pointed out by Garcia et al., there are slopes, and for this model, mass ratios, where dissipation occurs at foot-strike, but walking motions are unstable [7]. Thus, dissipation at foot-strike

does not guarantee orbital stability [3,7]. Dissipation at foot-strike, however, is required for existence of orbitally stable solutions for this hybrid continuous-discrete system. Since all swing phase solutions considered are locally (and orbitally) unstable, the discrete dynamics of the foot-strike event are the way solutions to the hybrid system become orbitally stable.

### 3.5. Equating local and orbital stability

To improve the understanding of the relationship between local and orbital stability, we calculate orbital stability for the hybrid continuous-discrete system from local stability measures. We borrow from Floquet theory for continuous periodic solutions, and extend the method to handle the walker dynamics, which include both a continuous swing-phase and a discrete foot-strike event. We first examine the continuous swing-phase dynamics. For a period-one walking solution with period  $T$ , an arbitrary perturbation at the beginning of swing (post-foot-strike) evolves to a perturbation at the end of swing (pre-foot-strike) by integrating the localized Jacobian, Eq. (10), along the equilibrium solution to yield an  $n$  by  $n$  map,  $\Phi_F(T)$ ,

$$\dot{\Phi}_F(t) = \mathbf{J}_F|_{s_{eq}(t)} \Phi_F(t) \quad \text{and} \quad \Phi_F(0) = \mathbf{I}. \quad (21)$$

This map, the state transition matrix (or fundamental matrix)  $\Phi_F(T)$ , maps initial to final perturbations over the swing-phase dynamics in the original Hamiltonian coordinate frame,

$$\delta(T) = \Phi_F(T) \delta(0). \quad (22)$$

Swing-phase ends only when the foot strikes the ground,  $\phi - 2\theta = 0$ . This must also hold for any perturbed solution,  $(\phi + \delta_\phi) - 2(\theta + \delta_\theta) = 0$ , thus,  $\delta_\phi - 2\delta_\theta = 0$ . In integrating Eq. (22), however, we have not imposed  $\delta_\phi - 2\delta_\theta = 0$  at foot-strike ( $t = T$ ). Furthermore, the stability of the orbital solution is independent of the amount that a perturbation simply advances or retards the solution in the tangent direction, i.e. phase-shift. These two observations may be accounted for by forming the following matrix,  $\mathbf{R}$ ,

$$\mathbf{R} = \mathbf{I} - \frac{\mathbf{F}(\mathbf{s}^-) \cdot \hat{\mathbf{n}}_\Sigma^T}{\mathbf{F}(\mathbf{s}^-)^T \cdot \hat{\mathbf{n}}_\Sigma} \quad (23)$$

where  $\mathbf{I}$  is the identity matrix,  $\mathbf{F}(\mathbf{s}^-)$  is the column  $n$ -vector tangent to the trajectory at  $\mathbf{s}^-$ , and  $\hat{\mathbf{n}}_\Sigma$  is a column  $n$ -vector normal to the Poincaré section,  $\Sigma$  [15]. We note that the Poincaré section and the hypersurface orthogonal to the tangent at foot-strike,  $\Gamma(T)$ , are only the same in the case that the tangent vector is orthogonal to the Poincaré section. The matrix  $\mathbf{R}$  is used to discard the evolution of perturbations in the tangent direction and retain only perturbation evolution in the three-dimensional Poincaré section,

$$\hat{\Phi}_F(T) = \mathbf{R} \cdot \Phi_F(T). \quad (24)$$

The matrix  $\hat{\Phi}_F(T)$  maps perturbations from the beginning to the end of the continuous swing-phase dynamics in the original position-momenta coordinate frame keeping only perturbations in  $\Sigma$ . To complete the orbit we need to apply the map for the foot-strike event from Eq. (17). Thus, the map from beginning of swing-phase for step  $i$  to the beginning of swing-phase for step  $i + 1$  is,

$$\Psi = D_s \mathbf{G}|_{s^-} \cdot \hat{\Phi}_F(T). \quad (25)$$

The matrix  $\Psi$  is the Jacobian of the Poincaré map for step  $i$  to  $i + 1$  and should be very similar to the numerical estimate of the Jacobian of the Poincaré map  $D_s \mathbf{P}|_{s_{eq}}$  from Eq. (8). Orbital stability is determined from the eigenvalues of  $\Psi$ . This method for determining the Jacobian of the Poincaré map has the

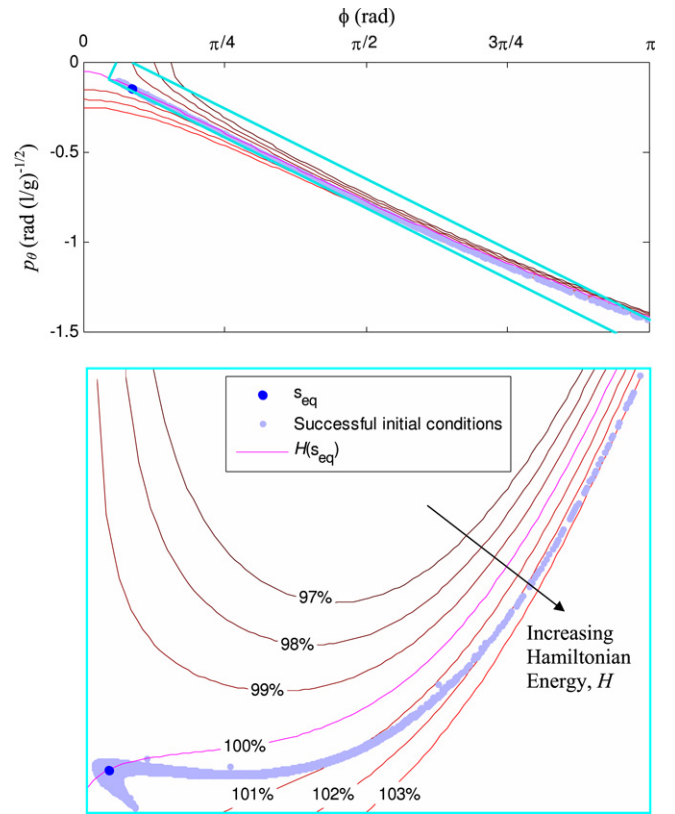


**Fig. 8.** The two-dimensional Poincaré section  $\Sigma$  at post-foot-strike states ( $p_\phi^+ = 0$ ) showing successful initial conditions for walking, which may also be thought of as the basin of attraction for the fixed point,  $s_{eq}$ . The slope,  $\gamma$ , was 0.003 radians and the mass ratio,  $\beta$ , was 0.02. All other initial conditions resulted in the walker “falling over”, i.e., the hip strikes the ground, or returning to the vertical standing posture (a static equilibrium point).

advantage that it is more robust to numerical error, because it avoids the problems associated with using small numerical perturbations [15].

We note that this procedure may also be applied when the solution is not periodic, and may be used to estimate Lyapunov exponents for systems that include continuous dynamics coupled with a discrete event applied at intersection with a Poincaré surface.

It is important to note that the local and orbital stability measures given here are only valid within an infinitesimal neighborhood of the fixed point. To examine the limits of nonlinear stability, in other words, the basin of attraction or passive recovery around the fixed point, we numerically explored the 2-dimensional space at the instant post-foot-strike by computing the solution from initial conditions in the region  $\phi \in (0, \pi)$  and  $p_\phi \in (0, -1.5)$ . Initial conditions that yielded solutions that returned to the fixed point, i.e. the basin of attraction, are shown as light-blue points in Fig. 8. There are two interesting observations. First, the basin of attraction is not constrained to a constant Hamiltonian energy. Second, although it appears that this region is discontinuous, we believe that it is only due to our discrete sampling precision. We chose to not sample higher, simply because our intent was to provide a qualitative image of the basin of attraction for the walking model. For more details on the basin of attraction for the simplest walking model, refer to [16].

## 4. Discussion

The passive walking cycle of the 2D walker demonstrates that stable walking motions are possible without active feedback control (neural or otherwise), and arise simply from the mechanical

properties of the system. Robotics researchers are currently trying to exploit this self-stabilization behavior seen in biology and some numerical models to design robots that require less energy to maintain stability [8,17]. For the 2D walker, examining local stability in the global state-basis resulted in an unstable direction throughout all of swing phase (Fig. 5). Using a time-varying rotation matrix, however, it is possible to uncouple the effects of perturbations that are tangent to the walking trajectory from evolution of the orthogonal directions. This is important because tangential perturbations only affect phase, i.e., they shift the solution along the unperturbed trajectory. Since tangential perturbations do not cause the solution to leave the unperturbed trajectory, they are not a concern when considering if a perturbation will result in the solution leaving the basin of attraction. In the case of the 2D walker where only one stable trajectory exists for a given parameter set, leaving the basin of attraction will result in the model falling over or converging on the steady state solution of standing. Only perturbations orthogonal to the periodic gait trajectory have the potential to cause the solution to leave the basin of attraction.

It is important to note that in contrast to the simple model explored here, in actual animal locomotion, perturbations along the trajectory may indeed affect the stability of a periodic gait. One hypothesis holds that periodic gaits are maintained via reference trajectory tracking, in which neural controllers command limbs to follow prescribed paths and sensory feedback activates muscles to maintain them [18]. Reference trackers seek to maintain a fixed phase relation of animal position with respect to the reference trajectory. Thus, perturbations away from the reference trajectory are countered not merely by convergence to any state-space point along the reference trajectory, but must converge to the cyclically moving reference point along the reference trajectory, i.e., converge to the correct phase in the gait cycle. Ignoring perturbations along the gait cycle would not be appropriate for such a system, but at this time it is not clear that animal locomotion operates by reference tracking, or some other process.

Nonetheless, understanding local stability has important implications in the design of controllers for bipedal locomotion. If a region in state-space along the gait cycle trajectory is locally stable, it may not be necessary for a controller to correct deviations – thus reducing the energy required to maintain stability. In regions of the state space where there are some directions that are locally stable, and some that are unstable, a control scheme could be devised that gives priority to correcting deviations in the unstable directions. In other words, a form of hierarchical control that applies control forces only when necessary would be advantageous over a system that attempts to control the trajectory everywhere in the state space.

In the biomechanics field, these techniques may be useful in understanding how our neuromuscular reflexes and the nonlinear behavior of our musculoskeletal system (i.e., reflexes) contribute to stability maintenance during walking and more general motor control.

Two other techniques for investigating stability of walking models that are complementary to the local stability analysis, are the basin of attraction, and the gait sensitivity norm. The basin of attraction is the set of all possible states that will converge to the nominal walking cycle [16]. Computing the basin of attraction is computationally expensive, and it is difficult to relate to real world disturbance rejection [10,19]. The gait sensitivity norm was recently introduced for measuring stability and has been demonstrated in actual robotics development. It quantifies how a set of disturbances affect a set of gait indicators. The choice of disturbances and gait indicators is left up to the designer. As an example, Hobbelen, et al. [10], varied a control parameter in a physical robot and calculated the gait sensitivity norm for how the robot would respond to varying floor height.

One of the limitations of analyzing stability in the rotating orthogonal hypersurface is that the eigenvalues of the reduced **B** matrix depend on the choice of generalized coordinates, even when the equations are expressed in canonical Hamiltonian form. It may be possible, however, to take advantage of this limitation by searching for a set of generalized coordinates that would achieve an additional goal, such as minimizing controller complexity.

We also presented how orbital stability may be calculated from the local measures for models that include both continuous and discrete dynamics. The advantage to calculating orbital stability in this semi-analytical manner is that it avoids numerical errors associated with using numerical perturbations to estimate the Jacobian of the Poincaré map.

In summary, we have presented techniques for studying the stability of walking models. The walking model showed that even though there are walking cycles that are stable overall, these cycles have regions during the continuous swing phase where perturbations will tend to diverge in the short-term (local instability). Thus, even though the complete continuous-discrete hybrid walking cycle may exhibit overall orbital stability, appropriately timed perturbations to the trajectory while it is in a region of local instability may cause the trajectory to leave the basin of attraction of the walking cycle, leading to a fall. Understanding local stability will therefore be useful for both designing controllers for legged robots, and studying how the neuromuscular system maintains stability.

## Acknowledgment

We dedicate this paper to the memory of Kevin P. Granata.

## References

- [1] T. McGeer, Passive dynamic walking, *Int. J. Robot. Res.* 9 (1990) 62–82.
- [2] A. Goswami, B. Espiau, A. Keramane, Limit cycles and their stability in a passive bipedal gait, *IEEE Int. Conf. Robotics Automat.* (1996) 246–251.
- [3] A. Goswami, B. Espiau, B. Thuilot, A Study of the passive gait of a compass-like biped robot: Symmetry and chaos, *Int. J. Robot. Res.* 17 (1998) 1282–1301.
- [4] B. Thuilot, A. Goswami, B. Espiau, Bifurcation and chaos in a simple passive bipedal gait, *IEEE Int. Conf. Robotics Automation* (1997) 792–798.
- [5] D.H. Gates, J.L. Su, J.B. Dingwell, Possible biomechanical origins of the long-range correlations in stride intervals of walking, *Physica A* 380 (2007) 259–270.
- [6] M. Kwan, M. Hubbard, Optimal foot shape for a passive dynamic biped, *J. Theoret. Biol.* 248 (2) (2007) 331–339.
- [7] M. Garcia, A. Chatterjee, A. Ruina, M. Coleman, The simplest walking model: Stability, complexity, and scaling, *J. Biomech. Eng.* 120 (1998) 281–288.
- [8] S. Collins, A. Ruina, R. Tedrake, M. Wisse, Efficient bipedal robots based on passive-dynamic walkers, *Science* 307 (2005) 1082–1085.
- [9] A.D. Kuo, Energetics of actively powered locomotion using the simplest walking model, *J. Biomech. Eng.* 124 (2002) 113–120.
- [10] D.G.E. Hobbelen, M. Wisse, A disturbance rejection measure for limit cycle walkers: The gait sensitivity norm, *IEEE Trans. Robot.* 23 (2007) 1213–1224.
- [11] F. Ali, M. Menzinger, On the local stability of limit cycles, *Chaos* 9 (1999) 348–356.
- [12] A.H. Nayfeh, B. Balachandran, *Applied Nonlinear Dynamics: Analytical, Computational, and Experimental Methods*, John Wiley & Sons, Inc., New York, 1995.
- [13] K.D. Mombaur, H.G. Bock, R.W. Longman, Stable, unstable and chaotic motions of bipedal walking robots without feedback, *IEEE Int. Conf. Control Oscillations Chaos* (2000) 282–285.
- [14] W.S. Koon, M.W. Lo, J.E. Marsden, S.D. Ross, Heteroclinic connections between periodic orbits and resonance transitions in celestial mechanics, *Chaos* 10 (2000) 427–469.
- [15] I.A. Hiskens, Stability of hybrid system limit cycles: Application to the compass gait biped robot, in: 40th IEEE Conf. on Decision and Control, 2001, pp. 774–779.
- [16] A.L. Schwab, M. Wisse, Basin of attraction of the simplest walking model, in: ASME 2001 Design Engineering Technical Conferences, 2001, pp. 1–9.
- [17] R. Pfeifer, M. Lungarella, F. Iida, Self-organization, embodiment, and biologically inspired robotics, *Science* 318 (2007) 1088–1093.
- [18] P. Holmes, R.J. Full, D. Koditschek, J. Guckenheimer, The dynamics of legged locomotion: Models, analysis, and challenges, *SIAM Rev.* 48 (2006) 207–304.
- [19] D.G.E. Hobbelen, M. Wisse, Limit cycle walking, in: M. Hackel (Ed.), *Humanoid Robots: Human-like Machines*, Itech, Vienna, 2007, pp. 277–294.